Science of the Total Environment xxx (2009) xxx–xxx

Contents lists available at ScienceDirect

Science of the Total Environment

journal homepage: www.elsevier.com/locate/scitotenv

Estimation of suspended sediment concentrations using Terra MODIS: An example from the Lower Yangtze River, China

J.-J. Wang *, X.X. Lu

Department of Geography, National University of Singapore, 10 Kent Ridge Crescent, 119260, Singapore

ARTICLE INFO

Article history:
Received 6 August 2009
Received in revised form 21 November 2009
Accepted 24 November 2009
Available online xxxx

Keywords:
Satellite remote sensing
Suspended sediment concentration (SSC) retrieval
Terra MODIS image
Turbid water
The Yangtze River

ABSTRACT

Traditional measurements of suspended sediment concentrations (SSC) through in-situ sampling in rivers are expensive and time-consuming to perform. Thus, these methods cannot provide continuous SSC records. Although remote sensing has been used for SSC estimation, little research has been undertaken on inland rivers, especially for highly turbid rivers like the Yangtze. Previous studies have proposed Landsat TM/ETM+ Band 4 as a spectral SSC indicator for the Yangtze, but its limitation on temporal resolution is insufficient for the study of dynamic changes of sediment. This paper presents a method of estimating SSC of the Yangtze at Jiujiang using time-series satellite data of high temporal resolution Terra MODIS. It was found that differences in water reflectance between Band 2 and Band 5 could provide relatively accurate SSC estimation even when in-situ atmospheric conditions were unknown. After cross-validation, mean absolute relative error (ARE) and relative root mean square error (RRMSE) were relatively low (*i.e.*, 25.5% and 36.5%, respectively). This empirical relationship was successfully applied to the estimation of SSC at Datong in the Lower Yangtze River, although the SSC values were generally underestimated. This study suggests that Terra MODIS could be used to estimate SSC in large turbid rivers, although some influencing factors require further study to improve the accuracy of SSC estimation.

1. Introduction

To study sediment-associated environmental changes such as alterations of river channel morphology, degradation of water quality and negative effects on aquatic ecology, it is necessary to accurately monitor transport and discharge of suspended matter in rivers (Schiebe et al., 1992; Collins and Walling, 2004; Ouillon et al., 2004). However, this task is constrained by severely limited spatial and temporal samplings of suspended sediment concentration (SSC) due to the high cost and time-consuming methods currently used for in-situ measurement (Gao and O'Leary, 1997). As Syvitski et al. (2000) indicated, most rivers in the world have either not been gauged or their sediment data are not readily available.

Satellite remote sensing has been used to retrieve SSC data because it has wide spatial coverage and high temporal repeatability, and various visible and NIR bands have been proposed as SSC indicators in previous studies (e.g., Ritchie and Cooper, 1988; Li, 1993; Reddy and Srinivasulu, 1994; Dekker et al., 2002; Doxaran et al., 2002; Ouillon et al., 2004; Chen et al., 2004; Wang et al., 2004; Milier and Mckee, 2004; Binding et al., 2005; Ma and Dai, 2005; Zhou et al., 2006). These studies have focused mainly on coastal, estuarine, lagoon, lake and reservoir environments. Previous studies on rivers, such as Islam et al. (2001) on the Ganges–Brahmaputra Rivers and Onderka and Pekarova (2008) on the Danube River, involved short river reaches within the coverage of a single Landsat image, and images from only one or two days were used. Moreover, these studies focused on moderately or mildly turbid waters. For instance, Onderka and Pekarova (2008) studied samples with 0–60 mg l^{-1} only. Islam et al. (2001) indicated that their algorithm was suitable for the SSC range of 0–1200 mg l^{-1}, but they used only five samples. Wang et al. (2007) found that SSC could be estimated from Landsat ETM+ images directly, and their study involved SSC samples within 22–2610 mg l^{-1} at 10 stations along the Upper Yangtze River. Wang et al. (2009) later used 16 ETM+ images covering 16 stations along the Upper and Middle Yangtze River to estimate SSC. Both studies found that the ETM+ Band 4 (NIR) was the best indicator of SSC.

Temporal resolution of Landsat TM and ETM+ is 16 days. Hence, to accurately monitor dynamic changes in a river system, higher temporal resolution images are required. Terra MODIS (or Moderate Resolution Imaging Spectroradiometer) may be a viable option. The Terra satellite was successfully launched on December 18, 1999, with Terra MODIS aboard (NASA MODIS Website, online: http://modis.gsfc.nasa.gov/index.php). Terra MODIS, passing from north to south across the equator in the morning, views the entire surface of the Earth every 1 or 2 days, acquiring data at 36 spectral bands within a range of 405–14,385 nm. Spatial resolutions are 250 m for Bands 1–2, 500 m for Bands 3–7 and 1000 m for Bands 8–36, respectively. Spatial resolutions of Bands 1–7 make them likely to be useful for large rivers such

* Corresponding author. Tel.: +65 65166135; fax: +65 67773091.
E-mail address: jianjunwang71@yahoo.com (J.-J. Wang).

0048-9697/$ – see front matter © 2009 Elsevier B.V. All rights reserved.
doi:10.1016/j.scitotenv.2009.11.057

as the Lower Yangtze. This study aimed to investigate whether Terra MODIS with higher temporal and spectral resolutions could be used to estimate SSC in a large river system.

2. Study area

The 6300 km-long Yangtze River, the third longest river in the world, originates in the Tibet Plateau and flows eastwards into the East China Sea (Fig. 1). The upper river reach covers an area 4500 km upstream to Yichang, Hubei Province, and the middle and lower reaches flow across a huge, gently sloping plain where the river channel widens. The middle and lower reaches of the river are dominated by a subtropical monsoon climate with a large proportion of annual precipitation in the wet season. The Three Gorges Dam (TGD), the largest dam in the world, is located 37 km upstream from Yichang (Nilsson et al., 2005). Due to the sediment deposition in this reservoir, SSC of water passing through the downstream main river channel has been declining since operation of the dam began in 2003 (Dai et al., 2008). Changes in sediment load along the Yangtze River may cause adverse environmental problems in the Middle and Lower Yangtze River basin, which is one of the most critical regions in China in terms of economic development. Along the Lower Yangtze River, Jiujiang and Datong are the only two gauging stations that measure sediment. Jiujiang is at the junction of the middle reach and the lower reach of the Yangtze River. Datong is the lowest station on the Yangtze River, so its sediment data were often used to estimate this large river's sediment flux into the sea. The channel width was around 1.5–2 km in wet seasons at Jiujiang and Datong, and the water depth was around 5–6 m at the two sites.

3. Data and methods

3.1. SSC data and Terra MODIS

At Jiujiang, the daily SSC data measured at gauging stations were point-integrated samples collected at 0.2, 0.6 and 0.8 water depths from ten verticals in the cross-section. The water samples were treated following the national standard (Ministry of Water Resources of China, 1992). The current study focused on the wet season (May–October) with tremendous temporal and spatial variations in SSC. The daily SSC ranged from 45 to 909 mg l^{-1} at Jiujiang during the entire wet season in 2005.

This study used geocoded Terra MODIS L1B images received by the Tokyo receiving station and the Bangkok receiving station, respectively. These geometrically corrected images were downloaded free from the MODIS Data Service Center website, Institute of Industrial Science, University of Tokyo, Japan (Online: http://webmodis.iis.u-tokyo.ac.jp/). Bands 1–7 were used in this study, and spatial resolutions at Bands 1–2 had been re-sampled to 500 m by the two receiving stations. MODIS images were checked before being downloaded to exclude cloudy days. Daily quick-look images are available at MODIS Rapid Response System of NASA (online: http://rapidfire.sci.gsfc.nasa.gov/realtime/?calendar).

3.2. Top-of-atmosphere (TOA) radiance and reflectance extraction

The pixels were selected according to the stations' geographic coordinates (Fig. 2). To facilitate selection of the pixels, Band 2 or band combination RGB = 765 was used for image display because it clearly

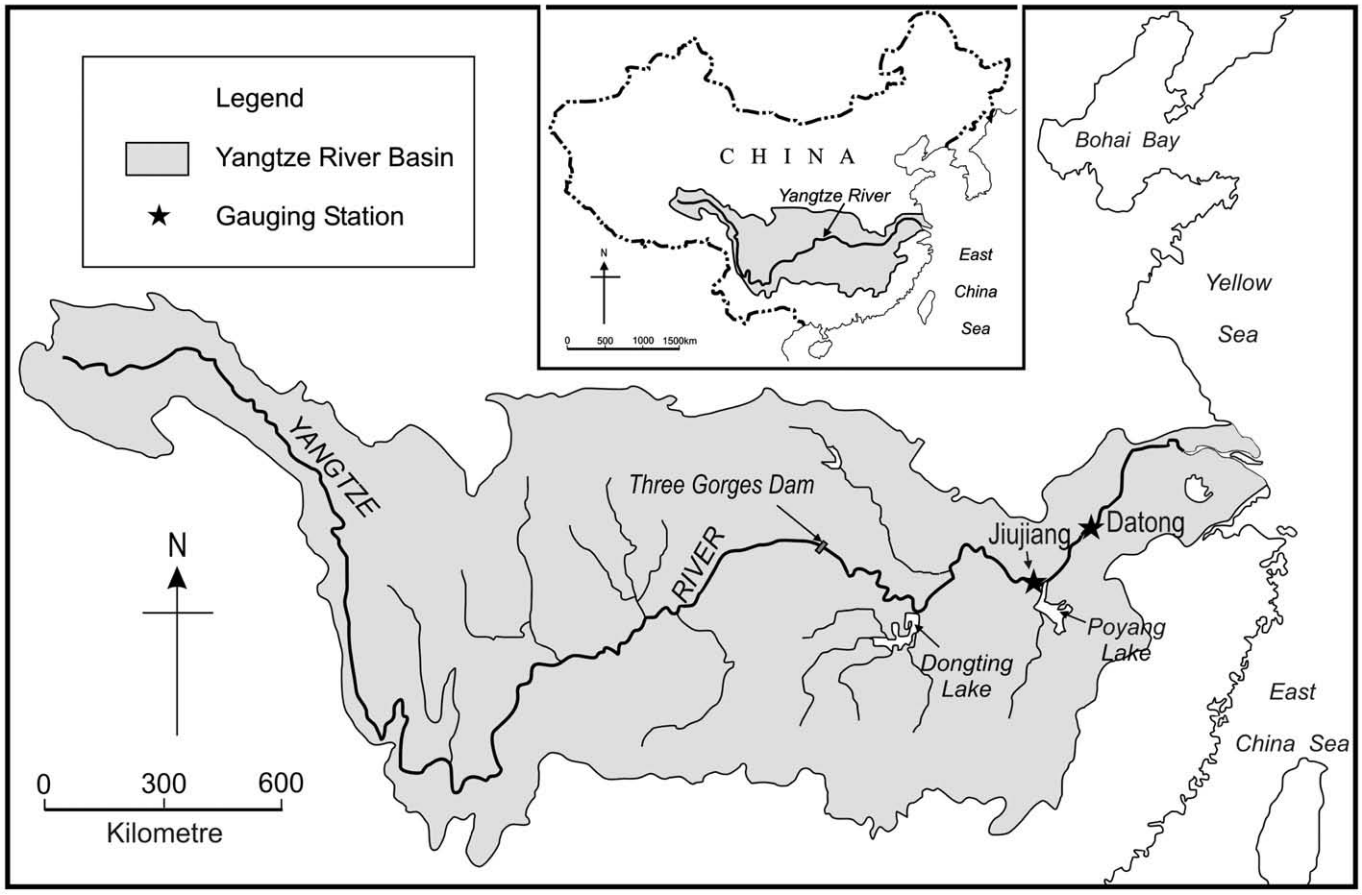

Fig. 1. Map of the Yangtze River basin showing the locations of Jiujiang and Datong, the only two gauging stations with sediment records along the Lower Yangtze River.

Please cite this article as: Wang J-J, Lu XX, Estimation of suspended sediment concentrations using Terra MODIS: An example from the Lower Yangtze River, China, Sci Total Environ (2009), doi:10.1016/j.scitotenv.2009.11.057

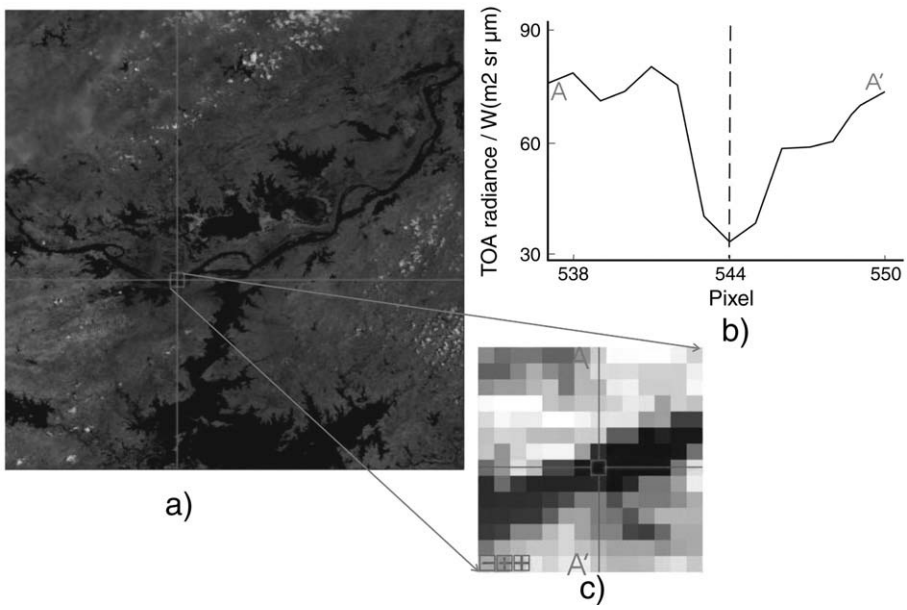

Fig. 2. Pixel selection and TOA radiance value determination at Jiujiang using MODIS Band 2 as an example. Limited by the river width and MODIS' spatial resolution, the pixel with the lowest TOA radiance at Band 2 was chosen. This MODIS image was acquired on July 3, 2005. Note that the contrast was enhanced in (c).

separates water bodies from land. Limited by the river width and the spatial resolution of MODIS, the pixel with the lowest TOA radiance at Band 2 was chosen because water radiance was significantly lower than land radiance in the studied river reach due to stronger absorption of water at Band 2. The TOA radiance of pixels was derived directly from the downloaded MODIS L1B data, and was then converted into TOA reflectance,

$$\rho_{i,\mathrm{TOA}} = \frac{\pi L_i d^2}{F_i \cos\theta_s} \quad (1)$$

where L_i is the at-sensor radiance, F_i is the mean TOA solar flux density, θ_s is the solar zenith angle and d^2 is the factor that corrects for the variation in solar irradiance due to the varying distance between the Earth and the Sun at different times of the year. The subscript i denotes the MODIS band number.

For river water, TOA reflectance at MODIS Band 7 (SWIR), denoted as $\rho_{7,\mathrm{TOA}}$, was used to represent contaminations of atmosphere and sun glint because of the very high absorption by water in SWIR region (Mobley, 1994). Without in-situ measurements of atmospheric conditions, this study used only the 35 samples at Jiujiang with lower $\rho_{7,\mathrm{TOA}}$ ($\leq$0.06). Among the 35 SSC samples, 34 samples ranged from 74 mg l^{-1} to 578 mg l^{-1}, and one sample had an SSC of 881 mg l^{-1}. Such SSC ranges are appropriate for Jiujiang, where the daily SCC ranged from 45 mg l^{-1} to 578 mg l^{-1} and from 579 mg l^{-1} to 909 mg l^{-1} during 95% and 5% of the total 184 days within the wet season of 2005, respectively. In addition, these SSC samples had good time coverage of the wet season of 2005 from the lowest to the highest water discharge (Fig. 3).

3.3. Atmospheric correction

To convert TOA reflectance to water reflectance, atmospheric effects must be corrected. Such a correction is quite difficult, especially when in-situ atmospheric conditions are unavailable. However, Wang et al. (2009) applied an atmospheric correction method without the requirement of in-situ atmospheric conditions. This method was found to be suitable for relatively clear views, especially for NIR bands where aerosol reflectance is expected to be small. Hence, Wang et al.'s method was also used in this study.

TOA reflectance at Bands 1–7 was first corrected for Rayleigh scattering and gaseous absorption to obtain the corrected reflectance (ρ^*) following Vermote and Tanré (1992) and Bird and Riordan (1984), and water reflectance was then estimated by subtracting ρ^* at Band 7 (SWIR) from ρ^* at Bands 1–6, respectively. More details about the principles and procedures of this method can be found in Wang et al. (2009).

3.4. Regression and validation

This study applied regression analysis to develop the SSC–reflectance relation at Jiujiang. Such regression relation was then validated using the leave-one-out cross-validation (LOOCV) technique. LOOCV has been used in remote sensing studies (e.g., Schlerf et al., 2005; Sterckx et al., 2007; Martin et al., 2008), because the predicted samples are different from the samples used to build the model. All 35 of the samples formed a calibration regression with Y (dependent variable) versus X (independent variable). To validate this regression, the first sample was excluded as a validation datum, and the other 34 were used as training data to develop a correlation between Y and X by a least squares regression. The slope, intercept and R^2 of the

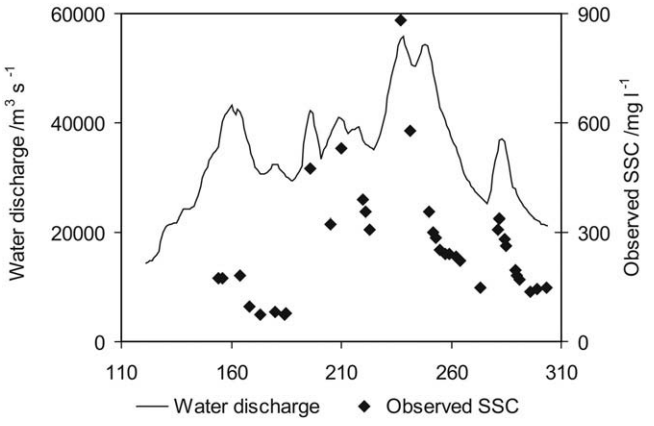

Fig. 3. Variations of daily water discharge and SSC in the wet season of 2005 at Jiujiang. SSC was lower in rising limb but higher in recession limb periods, showing a counterclockwise hysteresis effect. Note that the SSC was abnormal; specifically, it was lower in the first peak period.

Please cite this article as: Wang J-J, Lu XX, Estimation of suspended sediment concentrations using Terra MODIS: An example from the Lower Yangtze River, China, Sci Total Environ (2009), doi:10.1016/j.scitotenv.2009.11.057

resulting relation were recorded and then used to estimate Y of the excluded sample from X. This process was repeated by excluding all 35 samples, one by one. This produced a series of slope values, intercept values, R^2 values and estimated Y values, which were useful for assessing the accuracy of the calibration model.

Accuracy of SSC estimation was assessed by root mean square error (RMSE in mg l^{-1}), relative root mean square error (RRMSE in %) and absolute relative error (ARE in %). These were defined by:

$$RMSE = \sqrt{\frac{\sum_{i=1}^{n} (SSC_i - SSC_i')^2}{n}} \quad (2)$$

$$RRMSE = RMSE / \left(\frac{\sum_{i=1}^{n} SSC_i}{n} \right) \times 100\% \quad (3)$$

$$ARE = \left| \frac{SSC - SSC'}{SSC} \times 100\% \right| \quad (4)$$

where SSC_i refers to observed SSC_i, SSC_i' refers to estimated SSC_i, and $n = 35$.

The SSC–reflectance relation developed at Jiujiang was then applied to Datong to test whether it was also suitable for other sites along the Lower Yangtze River. RMSE, RRMSE and ARE were used to assess the accuracy of SSC estimation at Datong.

4. Results

4.1. Spectral signature of water samples

Atmospheric effects in TOA reflectance have been largely removed to retrieve water reflectance, especially at shorter wavelengths (Fig. 4). Retrieved water reflectance generally increased at Bands 1–6 with increasing SSC. Peak water reflectance appeared at Band 1 (red) for most samples. A spectral signature such as this is consistent with other studies (e.g., Ritchie et al., 1976; Forget et al., 1999).

Fig. 5 shows variations of water reflectance at Bands 1–6 (denoted as $\rho_{w,1} - \rho_{w,6}$, respectively) with SSC. The reflectance values of the two long-wavelength bands, $\rho_{w,5}$ and $\rho_{w,6}$, were small and did not have a close relation with SSC, possibly due to the residual atmospheric effects. On the other hand, $\rho_{w,3}$, $\rho_{w,4}$ and $\rho_{w,1}$ showed a positive relation with SSC, but the increase of reflectance with SSC became significantly slower when SSC was over 150 mg l^{-1}. Such saturation behaviour has been found in both laboratory experiments and field studies (e.g., Stumpf and Pennock, 1998; Bowers et al., 1989).

A linear relation appeared to describe the SSC–$\rho_{w,2}$ relation for the SSC less than 600 mg l^{-1}. However, the sample with 881 mg l^{-1} was below the regression line, so the SSC–$\rho_{w,2}$ relation was nonlinear for the larger SSC (Fig. 5). This was in agreement with previous studies. For example, Han and Rundquist (1994) reported that the SSC–reflectance relation for wavelengths of 700–900 nm was linear over the SSC range 50–600 mg l^{-1}, and the relation was nonlinear at higher SSC levels (600–1000 mg l^{-1}). In addition, as mentioned above, neither $\rho_{w,5}$ nor $\rho_{w,6}$ had a significant relation with SSC. Therefore, they were determined to mainly represent residual atmospheric effects (e.g., adjacency effects), because the impacts from chlorophyll and coloured dissolved organic matter are small (Sterckx et al., 2007) and the absorption by water is high (Mobley, 1994) at long-wavelength bands. Compared with Band 6, the residual atmospheric effect at Band 5 was closer to that at Band 2, because the residual atmospheric effect decreased with wavelength after correction by the method used in this study (Wang et al., 2009). Therefore, this study further minimised the residual atmospheric effect at Band 2 by subtracting $\rho_{w,5}$ from $\rho_{w,2}$.

4.2. Development of the SSC–water reflectance relation

Based on the above analysis, an empirical regression between ln-transformed SSC and $\rho_{w,2} - \rho_{w,5}$ was derived (Fig. 6a):

$$Y = 4.117 + 0.262 \times X (Y = \ln(\text{SSC in mg l}^{-1}); \quad X = \rho_{w,2} - \rho_{w,5} \text{ in percentage}; R^2 = 0.78; n = 35, p < 0.001) \quad (5)$$

At the level of significance (α) of 0.05, the calculated T-value (10.82) is greater than the upper critical value (2.03); hence, the null hypothesis that the regression coefficient is zero is rejected. At the same α, the correlation coefficient (R) of 0.88 is greater than the critical values of the correlation coefficient (0.33), so it can be assumed that a significant relationship exists between ln (SSC) and $\rho_{w,2} - \rho_{w,5}$.

This equation was validated using LOOCV. A series of intercept values (a), slope values (b) and R^2 values produced during iteration in LOOCV showed little variation. Values of a, b and R^2 varied from 4.07 to 4.18, 0.25 to 0.27 and 0.75 to 0.80 with corresponding standard deviations of 0.02, 0.00 and 0.01, respectively. In addition, the scatter plot of Fig. 6b compared the observed and the estimated SSC, and the points were well distributed along the 1:1 relationship. The residuals

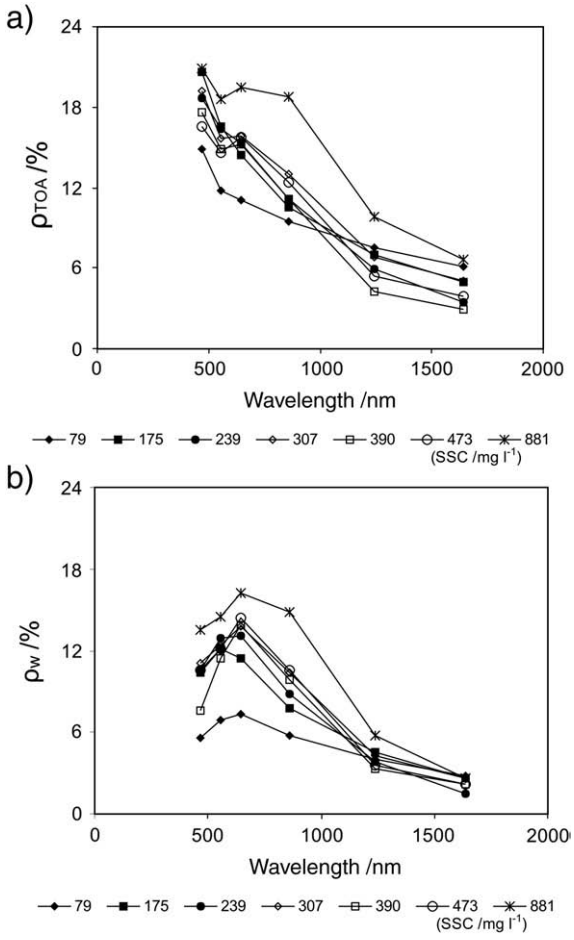

Fig. 4. Typical variations of TOA reflectance (a) and retrieved water reflectance (b) at Bands 1–6 with increasing SSC. The variable ρ_{TOA} is TOA reflectance, and ρ_w is water reflectance. Note that different symbols for data points along the lines represent different SSC values.

Please cite this article as: Wang J-J, Lu XX, Estimation of suspended sediment concentrations using Terra MODIS: An example from the Lower Yangtze River, China, Sci Total Environ (2009), doi:10.1016/j.scitotenv.2009.11.057

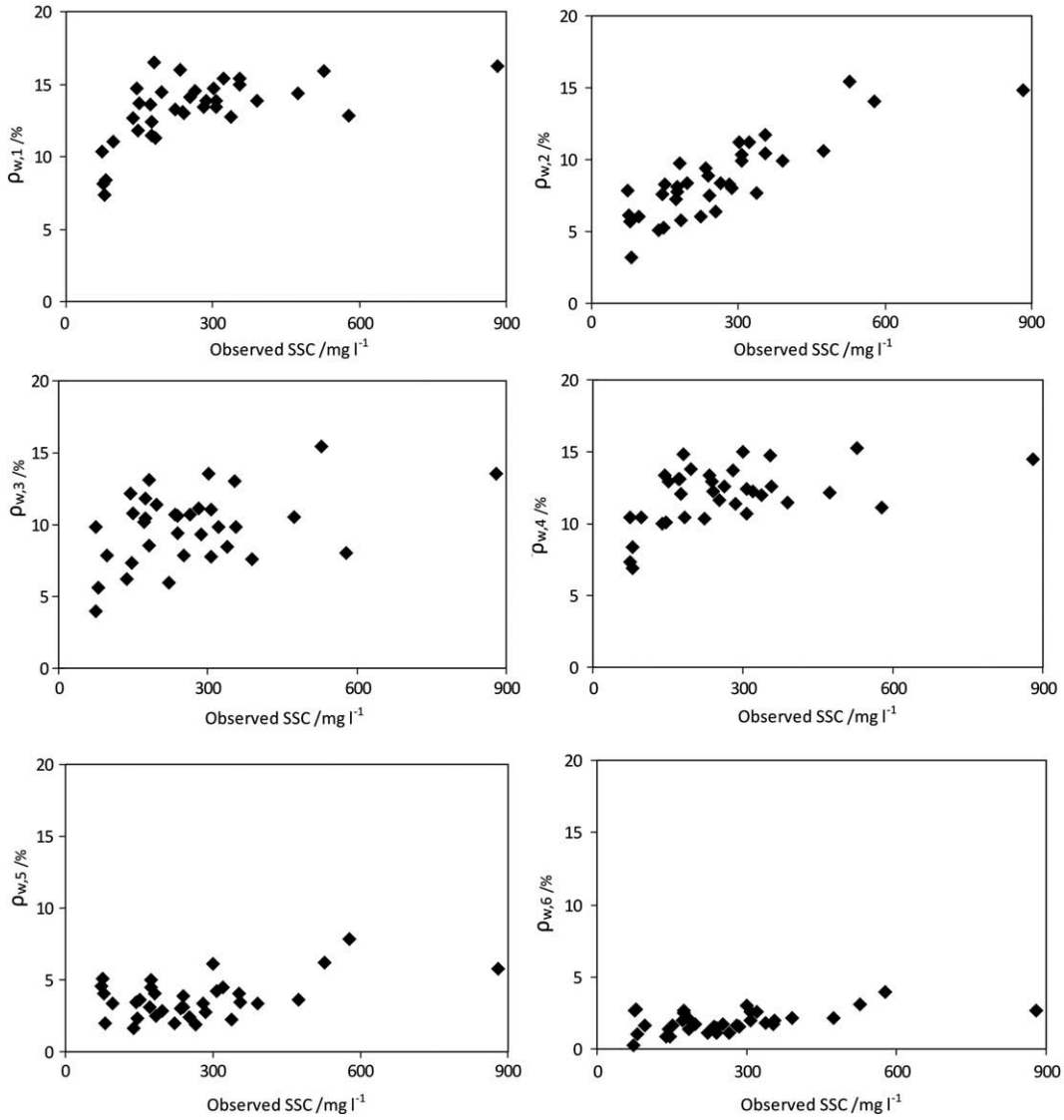

Fig. 5. Scatter plot of observed SSC against water reflectance (ρ_w) at Bands 1–6 in the Lower Yangtze River at Jiujiang. It appears that increase of reflectance with SSC became significantly slow when SSC was over 150 mg l^{-1} at Bands 1, 3 and 4 and, by contrast, when SSC was over 600 mg l^{-1} at Bands 2,

of ln (SSC) are distributed evenly in the region of ±0.4 (Fig. 6c). Mean ARE is 25.5% with an RMSE of 96.1 mg l^{-1} and an RRMSE of 36.5%. Fig. 6d displays variations in water discharge, as well as observed and estimated SSC with time. In comparison to previous studies, SSC estimation error of this study is much smaller. For example, in Doxaran et al.'s (2002) study of the Gironde estuary in southwest France, errors of SSC estimation from their empirical model varied from 32.9% to 38.2% (average value was 35.9%) for the SSC range of 38–2620 mg l^{-1}. However, caution should be taken when applying the regression relation of this study because on some days the residuals were much larger than on other days (Fig. 6).

4.3. Application of the empirical model to Datong

Previous studies applied regression to estimate SSC at other sites (e.g., Onderka and Pekarova, 2008). Wang et al. (2009) also found that an empirical regression was suitable for various sites along the Upper and Middle Yangtze River. It would be useful to test Eq. (5) at other sites along the Lower Yangtze River. Because Jiujiang and Datong are closer than those in Wang et al. (2009), the regression relation (Eq. (5)) was applied to the Datong station to estimate SSC from Terra MODIS images acquired in 2005. Fig. 7a compares the observed and the estimated SSC values, and the points are well distributed along the 1:1 relationship, although the higher SSC values were underestimated. Mean ARE was 19.8% with an RMSE of 63.0 mg l^{-1} and an RRMSE of 23.9%. Fig. 7c displayed the variations of the water discharge, as well as the observed and estimated SSC during the study period. It is noted that, in general, SSC was underestimated at Datong. This could be due to the errors discussed earlier, but the exact cause is unclear at this stage.

There are three sources of error. First, the Terra satellite circles around the Earth in a sun-synchronous orbit that descends across the equator at 10:30 a.m. local time. As for the time of SSC measurements, according to the Ministry of Water Resources of China (1992), "if the intra-daily SSC changes are periodic, the samples should be taken at a representative time determined by experiments". In general, the samples are taken at 8 a.m., 12 p.m. or 4 p.m. Hence, the temporal discrepancy between satellite overpass and timing of sediment collection may explain the error in SSC estimation in a situation where the intra-daily SSC changes are dramatic. Second, the particle size distribution can affect the SSC–reflectance relation because smaller sized sediments generally lead to a higher spectral reflectance for similar SSC (Bhagava and Mariam, 1991; Gin et al., 2003). Particle sizes of suspended sediments in the Yangtze River showed a positive

Please cite this article as: Wang J-J, Lu XX, Estimation of suspended sediment concentrations using Terra MODIS: An example from the Lower Yangtze River, China, Sci Total Environ (2009), doi:10.1016/j.scitotenv.2009.11.057

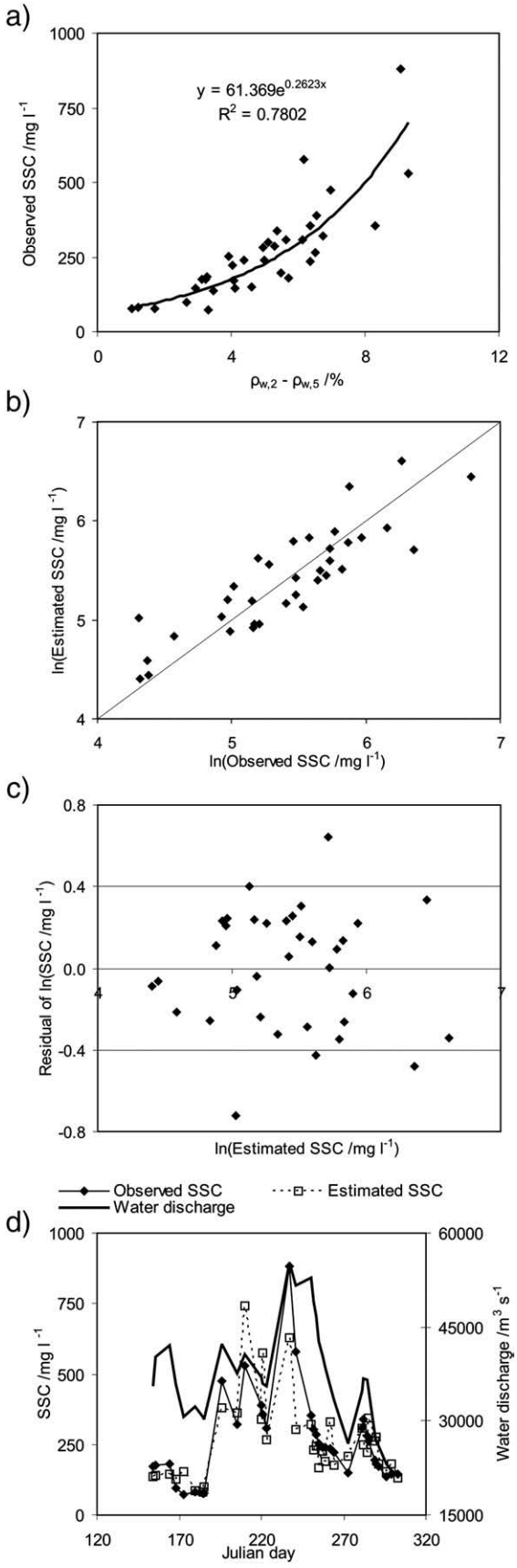

relation with water discharge according to Wu and Peng's (2005) study at Datong. Thus, the accuracy of Eq. (5) may vary with water discharges. Third, although the atmospheric correction procedure of this study worked effectively for the turbid waters where signals reflected by sediments were much stronger than residual atmospheric effects, the residual atmospheric effects still may reduce the accuracy of Eq. (5). This study involved MODIS data acquired during the period of 35 and 33 days at Jiujiang and Datong, respectively. The residual atmospheric effects were not the same at various days.

5. Discussion

5.1. Atmospheric correction

Reliable and robust atmospheric correction methods are required to ensure that the retrieved water reflectance values are comparable among a time-series of images (Ritchie et al., 1987; Tyler et al., 2006). This is particularly true for this study involving MODIS data acquired on 35 dates. Currently, no atmospheric correction method is strongly valid for highly turbid waters (Doxaran et al., 2009). The atmospheric correction method used in this study largely eliminated atmospheric effects from the satellite data (Fig. 4). It was found that the residual atmospheric effect at Band 2 could be further minimised by subtracting $\rho_{w,5}$ from $\rho_{w,2}$. This is consistent with Sterckx et al. (2007), who indicated that external effects such as adjacency influences and light reflection from the sky could be effectively corrected by subtracting the reflectance at 1004 nm from the reflectance at 833 nm.

In this study, the variation of retrieved water reflectance with increasing SSC was in line with previous studies. In Han's (1997) laboratory experiment, spectral reflectance increased with increasing SSC within the range 0–500 mg l^{-1} for wavelengths between 400 and 900 nm. Liew et al. (2003) reported that the reflectance in the red band to the NIR spectral region generally increased with increasing SSC within 16–1338 mg l^{-1}. Such consistencies showed that the atmospheric correction procedure used in this study worked effectively for the turbid waters where signals reflected by sediments were much stronger than residual atmospheric effects.

5.2. Optimal spectral indicator of SSC changes

The optimal wavelength used to measure substances (e.g., suspended solids, chlorophyll and yellow substance) in waters depends on some factors such as concentrations of these substances, characteristics of sensors and so on (Schmugge et al., 2002). Various bands and sensors have been proposed to estimate the SSC of water. Dekker et al. (2001) reported that Landsat TM Bands 2 (green)–3 (red) were suitable for estimating SSC for lake waters within SSC range 0–50 mg l^{-1}, and similarly Tyler et al. (2006) reported that Landsat TM Band 3 showed strong significant correlations with SSC of lake waters (SSC<60 mg l^{-1}). Binding et al. (2005) reported that a robust relationship was found between SSC (<25 mg l^{-1}) and reflectance in the red region in the Irish Sea. Sterckx et al. (2007) used NIR bands of the AHS sensor as a SSC indicator in an estuary (SSC: 0–400 mg l^{-1}). Harrington et al. (1992) reported that Landsat MSS Band 3 (NIR) was suitable for 0–500 mg l^{-1}, and MSS Band 4 (NIR) was suitable for higher SSC. In general, it seems that NIR bands are appropriate for higher SSC waters, whereas visible bands are appropriate for lower SSC waters.

Fig. 6. Detailed results of regression between SSC and the water reflectance difference between Band 2 and Band 5 ($\rho_{w,2}-\rho_{w,5}$) in the Lower Yangtze River at Jiujiang ($n=35$). (a) Regression relationship between SSC and $\rho_{w,2}-\rho_{w,5}$. (b) Comparison between ln-transformed observed and estimated SSC after leave-one-out cross-validation (the line shows a 1:1 relationship). (c) Residual of ln-transformed SSC versus ln-transformed estimated SSC. (d) Variations of water discharge, and observed and estimated SSC with time.

Please cite this article as: Wang J-J, Lu XX, Estimation of suspended sediment concentrations using Terra MODIS: An example from the Lower Yangtze River, China, Sci Total Environ (2009), doi:10.1016/j.scitotenv.2009.11.057

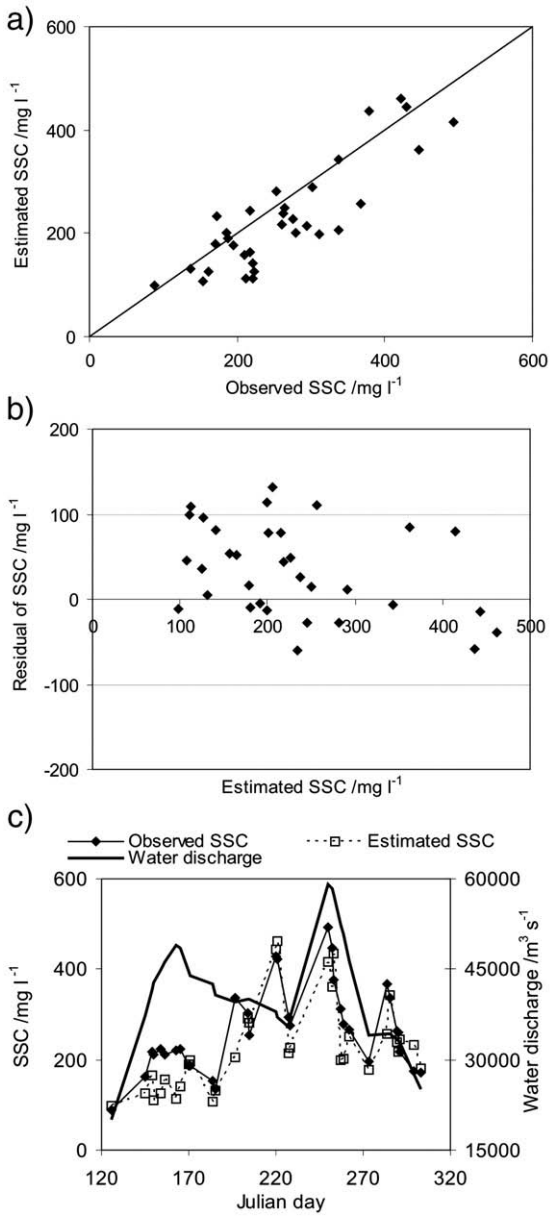

Fig. 7. (a) Scatter plot of observed SSC against estimated SSC of the Lower Yangtze River at Datong ($n=33$), where the line indicates a 1:1 relationship. (b) Residual of SSC versus estimated SSC. (c) Variations of water discharge, and observed and estimated SSC with time. The SSC was estimated from 33 MODIS images using the empirical model developed at Jiujiang.

This study found that $\rho_{w,2}$ (*i.e.*, retrieved water reflectance at MODIS Band 2) was a good SSC indicator after being subtracted by $\rho_{w,5}$ to further minimise the residual atmospheric effect. By contrast, visible bands showed quick saturation (Harrington et al., 1992; Wang et al., 2009). Besides, compared with visible bands, NIR bands have much less impact from chlorophyll and coloured dissolved organic matter (Sterckx et al., 2007). Han's (1997) laboratory experiment demonstrated that the effect of algae on the SSC–reflectance relation was minimal at wavelengths between 700 and 900 nm. Binding et al. (2005) indicated that the influence of the yellow substance was minimal at longer wavelengths. In addition, the atmospheric correction method used in this study likely works better in the NIR region than in the visible region because of higher aerosol scattering at short wavelengths (Wang et al., 2009), and thus retrieved water reflectance at visible bands may include higher contamination.

Both linear and nonlinear relations between SSC and reflectance have been proposed. This was mainly due to the SSC values. A nonlinear relation between water reflectance and SSC ranging from 22 to 2610 mg l^{-1} was reported for the turbid water in the Upper and Middle Yangtze River (Wang et al., 2007, 2009). However, this study found that water reflectance at MODIS Band 2 showed a linear relationship with SSC within the range of 74–600 mg l^{-1} and a nonlinear relationship within the range of 600–881 mg l^{-1}. Harrington et al. (1992) reported that reflectance at Landsat MSS 3 (NIR) had a linear relationship with SSC within the range of 0–500 mg l^{-1}, but the relationship became nonlinear when SSC increased further.

In addition to single bands, reflectance ratios between the NIR and visible bands (red, green and blue), as well as the ratio of the red band to the green band, have also been proposed to indicate SSC (Topliss et al., 1990; You and Hou, 1992; Doxaran et al., 2009). Doxaran et al. (2002) pointed out that use of reflectance ratios could reduce sky light reflection and the influence of particle grain-size and refractive index variations. However, Binding et al. (2005) argued that reflectance ratios worked well only for highly turbid waters where scattering is sufficient to overcome the strong absorption by other optically active materials in water at these wavelengths. In this study, band ratios did not show a good regression relation with SSC. A possible reason may be that atmospheric correction was not as effective at visible bands as at the NIR band, such that more residual atmospheric effects remained in the shorter wavelength bands.

5.3. Significance of MODIS-based SSC estimation

In comparison to Landsat, MODIS could provide more frequent information on sediment because of its much higher temporal resolution. For example, only one ETM+ image is available per 16 days, whereas nearly 16 MODIS images are available during the same period. Furthermore, only a few ETM+ images are cloud-cover-free, while dozens of MODIS images were relatively clear in the one-year period of the study area according to our experience. On the other hand, it must be noted that MODIS data may be unsuitable for relatively narrow channels such as the Upper Yangtze reach because of MODIS' spatial resolution.

If more frequent SSC data can be estimated for the days without sediment measurements, MODIS images may also be useful for estimating annual sediment fluxes in rivers jointly with a rating curve that represents the regression relation between SSC and water discharge (Horowitz, 2003). To achieve this, at least 20 SSC samples covering a broad range of SSC are required to build a reliable rating curve (Walling, 2005). This study demonstrates that a total of 35 and 33 relatively clear views of MODIS were available in 2005 at Jiujiang and at Datong, respectively. Therefore, a large number of archived MODIS images have the potential to provide much information on riverine SSC.

6. Conclusions

Effective atmospheric correction is extremely difficult to achieve, especially when in-situ atmospheric conditions are unknown, but it is required for the analysis of multi-dated images. To reduce the difficulty of atmospheric correction, this study excluded those images with higher atmospheric contaminations using a filter: $\rho_{7,TOA}>0.06$. For the relatively clear views, the atmospheric correction method used appeared to provide effective corrections, especially at the NIR bands, for MODIS images acquired on up to 35 dates at Jiujiang and 33 dates at Datong throughout the entire wet season of 2005.

This study found that the reflectance difference between Band 2 and Band 5 showed a significant logarithm relationship with SSC at Jiujiang. The regression relationship was validated by LOOCV, resulting in a relatively low mean ARE of 25.5% and RRMSE of 36.5%. Due to its higher temporal resolutions, MODIS can provide much more

Please cite this article as: Wang J-J, Lu XX, Estimation of suspended sediment concentrations using Terra MODIS: An example from the Lower Yangtze River, China, Sci Total Environ (2009), doi:10.1016/j.scitotenv.2009.11.057

frequent information on SSC variations than Landsat. This makes it possible to estimate annual sediment fluxes jointly with the rating curve method. Such information is critical in the field of fluvial geomorphology and hydrology to better understand dynamic changes in a river system. Nevertheless, it should be noted that this does not imply that the regression relation of this study is necessarily suitable for other years. For example, some large dams like the Three Gorges Dam could significantly change the particle size of suspended sediments.

The regression relationship developed at Jiujiang was found to be suitable for SSC retrieval at Datong with mean ARE of 19.8% and RRMSE of 23.9%. Further efforts will focus on whether this relationship can also be found in sites along the Middle Yangtze River. If this relationship is validated in the Middle Yangtze River, MODIS data may provide SSC estimates for the entire Middle and Lower Yangtze River, which would be of major importance for the investigation of spatial SSC variations along the river channel as well as identification of sediment sources.

Acknowledgements

This research was funded by the National University of Singapore (grant number R-109-000-086-646). The authors would like to extend their appreciation and thanks to Dr Chang Chew Wai at CENSAM IRG, SMART, MIT, Singapore, for his advice on atmospheric correction, and to Dr Vivarad Phonekeo at NOAA-MODIS Receiving Stations, Geoinformatics Center (GIC), Asian Institute of Technology (AIT), Thailand, and Dr Wataru Takeuchi at MODIS Data Service Center, Institute of Industrial Science, University of Tokyo, Japan, for their help in downloading MODIS images. Thanks are given to the three anonymous reviewers whose comments improved the manuscript.

References

Bhagava DS, Mariam DW. Effects of suspended particle-size and concentration on reflectance measurements. Photogr Eng Remote Sens 1991;57:519–29.
Binding CE, Bowers DG, Mitchelson-Jacob EG. Estimating suspended sediment concentrations from ocean colour measurements in moderately turbid waters; the impact of variable particle scattering properties. Remote Sens Environ 2005;94:373–83.
Bird RE, Riordan C. Simple solar spectral model for direct and diffuse irradiance on horizontal and tilted planes at the earth's surface for cloudless atmospheres. Technical Report No. SERI/TR-215-2436. Golden, CO: Solar Energy Research Institute; 1984.
Bowers DG, Boudjelas S, Harker GEL. The distribution of fine suspended sediments in the surface waters of the Irish Sea and its relation to tidal stirring. Int J Remote Sens 1989;19(14):2789–805.
Chen XL, Li YS, Liu ZG, Yin KD, Li ZL, Wai WH, et al. Integration of multi-source data for water quality classification in the Pearl River estuary and its adjacent coastal waters of Hong Kong. Cont Shelf Res 2004;24(16):1827–43.
Collins AL, Walling DE. Documenting catchment suspended sediment sources: problems, approaches and prospects. Prog Phys Geogr 2004;28:159–96.
Dai SB, Lu XX, Yang SL, Cai AM. Impact of human activities and natural processes on the river sediment discharge into the sea: an integrated study on the Yangtze River, China. Quatern Int 2008;186:43–54.
Dekker AG, Vos RJ, Peters SWM. Comparison of remote sensing data, model results and in situ data for total suspended matter (TSM) in the southern Frisian lakes. Sci Total Environ 2001;268:197–214.
Dekker AG, RJ VOS, Peters SWM. Analytical algorithms for lake water TSM estimation for retrospective analyses of TM and SPOT sensor data. Int J Remote Sens 2002;23:15–35.
Doxaran D, Froidefond JM, Lavender S, Casting P. Spectral signature of highly turbid waters: application with SPOT data to quantify suspended particulate matter concentrations. Remote Sens Environ 2002;81:149–61.
Doxaran D, Froidefond JM, Castaing P, Babin M. Dynamics of the turbidity maximum zone in a macrotidal estuary (the Gironde, France): observations from field and MODIS satellite data. Estuar Coast Shelf Sci 2009;81:321–32.
Forget P, Ouillon S, Lahet F, Broche P. Inversion of reflectance spectra of non-chlorophyllous turbid coastal waters. Remote Sens Environ 1999;68:264–72.
Gao J, O'Leary SM. Estimation of suspended solids from aerial photographs in a GIS. Int J Remote Sens 1997;18(10):2073–86.
Gin KYH, Koh ST, Lin II. Spectral irradiance profiles of suspended marine clay for the estimation of suspended sediment concentration in tropical waters. Int J Remote Sens 2003;24(16):3235–45.
Han L. Spectral reflectance with varying suspended sediment concentrations in pure and algal-laden waters. Photogr Eng Remote Sens 1997;63(6):701–5.
Han L, Rundquist DC. The response of both surface and underwater light field to various levels of suspended sediments: preliminary results. Photogr Eng Remote Sens 1994;60(12):1463–71.
Harrington JA, Schiebe FR, Nix JF. Remote sensing of Lake Chicot, Arkansas: monitoring suspended sediments, turbidity, and secchi depth with Landsat MSS data. Remote Sens Environ 1992;39:15–27.
Horowitz AJ. An evaluation of sediment rating curves for estimating suspended sediment concentrations for subsequent flux calculations. Hydrol Process 2003;17:3387–409.
Islam MR, Yamaguchi Y, Ogawa K. Suspended sediment in the Ganges and Brahmaputra Rivers in Bangladesh: observation from TM and AVHRR data. Hydrol Process 2001;15:493–509.
Li X. A united model for quantitative remote sensing of suspended sediment concentration. Int J Remote Sens 1993;14(14):2665–76.
Liew SC, Lu XX, Chen P, Zhou Y. Remote sensing estimation of suspended sediment concentrations in highly turbid inland river waters: an example from the Lower Jinsha Tributary, Yunnan, China. International Symposium on Remote Sensing of Environment, November 2003, Hawaii, USA; 2003.
Ma R, Dai J. Investigation of chlorophyll-a and total suspended matter concentrations using Landsat ETM and field spectral measurement in Taihu Lake, China. Int J Remote Sens 2005;26(13):2779–87.
Martin ME, Plourde L, Smith ML, Ollinger SV. A generalizable method for remote sensing of canopy nitrogen across a wide range of forest ecosystems. Remote Sens Environ 2008;112:3511–9.
Milier RL, Mckee BA. Using MODIS Terra 250 m imagery to map concentrations of total suspended matter in coastal waters. Remote Sens Environ 2004;93:259–66.
Ministry of Water Resources of China. Code for river suspended sediment measurement (GB 50159-92). Beijing: China Planning Press; 1992.
Mobley CD. Light and water: radiative transfer in natural waters. San Diego, CA: Academic Press; 1994.
Nilsson C, Reidy CA, Dynesius M, Revenga C. Fragmentation and flow regulation of the world's large river systems. Science 2005;308:405–8.
Onderka M, Pekarova P. Retrieval of suspended particulate matter concentrations in the Danube River from Landsat ETM data. Sci Total Environ 2008;397(1–3):238–43.
Ouillon S, Douillet P, Andrefouet S. Coupling satellite data with in situ measurements and numerical modeling to study fine suspended-sediment transport: a study for the lagoon of New Caledonia. Coral Reefs 2004;23:109–22.
Reddy MA, Srinivasulu S. Comparison of IRS-IB LISS-IIA pixel array sizes for estimating suspended solids concentration in Hussain Sagar Lake, Hyderabad, India—a statistical approach. Int J Remote Sens 1994;15:3693–706.
Ritchie JC, Cooper CM. Comparison of measured suspended sediment concentration with suspended sediment concentrations estimated from Landsat MSS data. Int J Remote Sens 1988;9(3):379–87.
Ritchie JC, Schiebe FR, McHenry JR. Remote sensing of suspended sediment in surface water. Photogr Eng Remote Sens 1976;42:1539–45.
Ritchie JC, Cooper CM, Jiang Y. Using Landsat multispectral scanner data to estimate suspended sediments in Moon Lake, Mississippi. Remote Sens Environ 1987;23:65–81.
Schiebe FR, Harrington Jr JA, Ritchie JC. Remote sensing of suspended sediments: the Lake Chicot, Arkansas project. Int J Remote Sens 1992;13:1487–509.
Schlerf M, Atzberger C, Hill J. Remote sensing of forest biophysical variables using HyMap imaging spectrometer data. Remote Sens Environ 2005;95:177–94.
Schmugge TJ, Kustas WP, Ritchie JC, Jackson TJ. Remote sensing in hydrology. Adv Water Resour 2002;25:1367–85.
Sterckx S, Knaeps E, Bollen M, Trouw K, Houthuys R. Retrieval of suspended sediment from advanced hyperspectral sensor data in the Scheldt estuary at different stages in the tidal cycle. Mar Geod 2007;30(1–2):97-108.
Stumpf RP, Pennock JR. Calibration of a general optical equation for remote sensing of suspended sediments in a moderately turbid estuary. J Geophys Res 1998;94:14363–71.
Syvitski JP, Morehead MD, Bahr DB, Mulder T. Estimating fluvial sediment transport: the rating parameters. Water Resour Res 2000;36:2747–60.
Topliss BJ, Amos CL, Hill PR. Algorithms for remote sensing of high concentration, inorganic suspended sediment. Int J Remote Sens 1990;11:947–66.
Tyler AN, Svab E, Preston T, Presing M, Kovacs WA. Remote sensing of the water quality of shallow lakes: a mixture modelling approach to quantifying phytoplankton in water characterized by high-suspended sediment. Int J Remote Sens 2006;27(8):1521–37.
Vermote EF, Tanré D. Analytical expressions for radiative properties of planar Rayleigh scattering media including polarization contribution. J Quant Spectrosc Radiat Transfer 1992;47(4):305–14.
Walling, D.E., 2005. Evaluation and analysis of sediment data from the Lower Mekong River, Report prepared for the Mekong River Commission, 61 pp.
Wang Y, Xia H, Fu J, Sheng G. Water quality change in reservoirs of Shenzhen, China: detection using Landsat TM data. Sci Total Environ 2004;328:195–206.
Wang JJ, Lu XX, Zhou Y. Retrieval of suspended sediment concentrations in the turbid water of the Upper Yangtze River using Landsat ETM+. Chin Sci Bull 2007;52 (supplement 2):273–80.
Wang JJ, Lu XX, Liew SC, Zhou Y. Retrieval of suspended sediment concentrations in large turbid rivers using Landsat ETM+: an example from the Yangtze River, China. Earth Surf Proc Land 2009;34:1082–92.
Wu YY, Peng LG. Relationships between suspended sediment size, water discharge and sediment concentration at Datong Gauging Station of the Yangtze River (in Chinese). J Sediment Res 2005;1:26–32.
You Y, Hou M. Remote sensing analysis of the suspended sediment transport in Lingdingyang. China Ocean Eng 1992;6:331–49.
Zhou W, Wang S, Zhou Y, Troy A. Mapping the concentrations of total suspended matter in Lake Taihu, China, using Landsat-5 TM data. Int J Remote Sens 2006;27(6):1177–91.

Please cite this article as: Wang J-J, Lu XX, Estimation of suspended sediment concentrations using Terra MODIS: An example from the Lower Yangtze River, China, Sci Total Environ (2009), doi:10.1016/j.scitotenv.2009.11.057